EPJ manuscript No.
(will be inserted by the editor)

Simulations of Microscopic Propulsion of Soft Elastic Bodies

David Urbanik[1], Shikhar Mani Dwivedi[2], and Colin Denniston[2,3]

[1] Cheriton School of Computer Science, The University of Waterloo
[2] Department of Applied Mathematics, The University of Western Ontario
[3] Department of Physics and Astronomy, The University of Western Ontario

January 10, 2018

Abstract. Using simulations that realistically model both hydrodynamic and elastic behavior, we study the motion of a microscopic, driven elastic sphere immersed in water. We first confirm the "jittery" relaxation recently predicted theoretically for an externally driven elastic sphere. The sphere is then divided in two and each section is driven internally with the two sections 180° out of phase. With periodic and perfectly symmetric driving, the elastic sphere spontaneously breaks symmetry and can attain macroscopic average swimming velocities to the right or left, the direction depending only on the initial state. With asymmetric driving the elastic sphere swims in one direction and the maximum speed is obtained with a 1/3:2/3 split. At high drive frequencies close to elastic resonances of the sphere, the motion can be quite efficient. At low drive frequencies the propulsion speed becomes independent of the elastic constants of the sphere and less efficient, but still substantial. Inertia is found to be an important driver of the behavior despite the small size of the spheres. As we model the full three-dimensional elasticity and compressible hydrodynamics, our simulations give not just qualitative indications but quantitative predictions for the motion.

PACS. XX.XX.XX No PACS code given

1 Introduction

Understanding the behavior of microscopic particles suspended in a fluid has increasingly many applications [12, 27–29, 14, 7, 21, 26] in the biological, chemical, and physical sciences. Recent work has shown that a number of interesting phenomena in microfluidics depend on inertia[7], something often assumed to be negligible for microscopic objects at small Reynolds number $\mathcal{R}$. For example, in the Stokes approximation (ignoring inertia) a microscopic particle in Poiseuille flow in a microfluidic channel should follow whatever streamline it is initially found on. This, however, does not occur [35]: the particles undergo *inertial* migration across streamlines to select a specific radial location [14]. The effect of fluid inertia on the microscale is not just an academic argument; it has real applications to microfluidics [7] and has been used for things such as inertial focusing and separation of particles by shape [26].

The origin of the conflict with what one would expect from estimates of the relative importance of the terms in Navier-Stokes equations lies in the power-law tails in the time correlation functions for small particles in a fluid [2, 42]. As a result, there is no time scale T where one can definitely ignore the effects of what has gone on before. It is only when the density of the particle is much greater than that of fluid can one typically ignore this behavior [13].

Send offprint requests to:

Normally, self-propelled microscopic biological or biologically inspired entities [8, 34, 17] swim slowly and follow constraints based on the Scallop Theorem[33], which places limitations on the mechanisms of propulsion available. However, artificial entities are not under the same biological constraints (for instance, they can be driven via an external field at potentially very high frequencies [11] and are not necessarily in a confined environment which will cut-off the power-law tails of the time correlation function) and it is worth investigating the full scope of modes of propulsion for such systems. Another key factor in the assumptions underlying the Scallop Theorem is that the object in question does not have any meaningful internal behavior, and so one can expect that the boundary behaviour alone is enough to describe the system. For extended elastic objects this is not the case [19]. Macroscopic swimmers, such as fish, are known to tune their body stiffness to optimize swimming speed [37] and actuating motion at the resonant frequency of the flexible body can dramatically increase the distance traveled per cycle [38]. Indeed, elastic materials have additional *internal* degrees of freedom which are independent of the exterior fluid flow, and can be used to store inertia during part of a periodic cycle and release it later to advance the state of the system.

Here, we demonstrate that driving a soft elastic body in a reciprocal manner almost invariably leads to a non-reciprocal motion that allows the body to build up non-negligible inertia. At low frequencies of the drive, the body

eventually settles to an average velocity that is independent of most of its internal properties (other than its size).

Recent theoretical work by Felderhof [9] found that the velocity relaxation of an elastic sphere immersed in a viscous incompressible fluid is "jittery": after a sudden external impulse a sufficiently flexible sphere will undergo many reversals of velocity. We first confirm this jittery relaxation is present in a numerical simulation of an elastic sphere in a viscous nearly incompressible fluid when the sphere is driven by an external force. When driven with a periodic external force, the response is found to be rarely in phase with the drive. We then split the sphere into two sections and drive them internally with the drive in the two sections 180° out of phase. In addition to oscillatory motion, the sphere obtains a net velocity, even when the two sections of the sphere are perfectly symmetric. This is somewhat surprising considering that there is nothing in the construction that favors going to the left or right and the drive is symmetric under time-reversal. However, the elastic response of the sphere to the drive is not symmetric under time reversal and the sphere spontaneously breaks the left-right symmetry and can go to the left or right depending only on the initial phase of the drive. This dependence on initial conditions implies that the inertial terms in the equations of motion are clearly important here, despite the small size of the spheres.

In this paper, we model a microscopic elastic particle with a large number of internal degrees of freedom. When driven at high frequencies near its elastic resonance the motion can be very efficient and even at low frequencies the body attains a steady speed independent of its internal details. There are a number of potential practical applications of such a system. As a sphere has the optimum surface to volume ratio it is the ideal shape to deliver a payload (inside its volume) to a given location with the minimum of extraneous extra material (such as a flagella) which would need to be discarded after delivery of a payload such as a drug. In the next section we outline the numerical model used for the simulations. Then in Section 3 we examine the externally driven elastic sphere and its jittery relaxation. In Section 4 we internally drive two sections of the sphere out of phase and study the resulting motion.

2 Model

To model a body with suitable elastic behaviour at the microscopic scale, it is natural to choose a spherical object as a starting point. As mentioned above there are practical applications of a spherical swimmer, but also the possibility that such a simple shape may have results that may be fully understood, as epitomized by the "spherical cow model". In our case, we simulated spherical objects 4 μm, and 10 μm in diameter. The sphere was placed in a square box with periodic boundary conditions in the x and y directions and fixed walls in the z direction (with no-slip boundary conditions at the walls). The presence of walls is necessary to break Galilean invariance and ensure that the fluid has a stationary reference frame (i.e. otherwise the fluid would just "catch-up" to a moving particle). The box side was four times larger than the particle diameter. The fluid density and viscosity were set to that of water (1 g/cm^3 and 1 centipoise respectively).

The simulation was performed using the LAMMPS[32] molecular simulation software, and the lb/fluid fix[24] implementing the Lattice-Boltzmann algorithm was used to simulate the fluid portion of the model. To model the interaction of the fluid with the the sphere, the lb/viscous fix[24] was used to add hydrodynamic forces to the outer layer of spherical particles[23,31]. The package uses a discretized version of the Boltzmann equation to solve for the fluid motion governed by the Navier-Stokes equations,

$$\begin{aligned} \partial_t \rho + \partial_\beta (\rho v_\beta) &= 0 \\ \partial_t (\rho v_\beta) + \partial_\beta (\rho v_\alpha v_\beta) &= -\partial_\alpha p + f_\alpha + \\ &\quad \eta \partial_\beta (\partial_\alpha v_\beta + \partial_\beta v_\alpha), \end{aligned} \tag{1}$$

on a uniform grid where ρ is the fluid density, $\mathbf{v}$ is the local fluid velocity, p is the pressure, set to $\rho/3(\Delta x^2/\Delta t^2)$, $\mathbf{f}$ is a local, external force resulting from the presence of the elastic particle, and η is the shear viscosity. We used $\Delta x = 0.564$ μm (1.41 μm) for the LB grid spacing for the 4 μm (10 μm) sphere, and a timestep of $\Delta t = 0.04$ μs for both.

The spheres were constructed with 856 constituent particles arranged in an hcp lattice connected by harmonic bonds between nearest neighbors with potential function

$$V(r) = \frac{1}{2} k (r - r_0)^2, \tag{2}$$

where k is the harmonic bond coefficient, r is the distance from a particle to its neighboring bonded atom, and r_0 is the equilibrium intermolecular distance ($r_0 = 1$ μm for the 10 μm sphere and $r_0 = 0.4$ μm for the 4 μm sphere). The nodes constituting the particle enables it to be modeled off lattice, using molecular dynamics techniques in LAMMPS[32]. Using standard analysis of harmonic crystals [5], it is possible to show that the bulk modulus of such a hcp crystal is $B = \frac{\sqrt{8}}{3} \frac{k}{r_0}$. We used this formula to compute k for a given value of B. To exhibit a range of behaviour and show how the motion of our spherical object varies with its elasticity, tests were conducted using elastic bulk moduli $B = 18.8$ kPa and $B = 1.88$ kPa, which span the range of elasticity from muscle tissue[6] on the high end to liver tissue[40] on the low end. The mass of each of the constituent particles was set so that the overall density of the elastic spheres was 1 g/cm^3, which puts the mass of the sphere with 10 μm diameter, at around 0.524 ng, and is comparable to the mass of an average E.Coli baterium [20].

We can define the *Reynolds Number*, the ratio of inertial forces to viscous forces, as

$$\mathcal{R} = \frac{\rho \mathrm{v} a}{\eta}, \tag{3}$$

where a is a characteristic size and v a characteristic velocity. Alternatively, the *Stokes Number*, the ratio of the

unsteady $\partial v/\partial t$ term to viscous forces, is

$$\mathcal{S} = \frac{\rho a^2}{\eta T}, \tag{4}$$

where T is a characteristic time. In many cases v $\approx a/T$ so that $\mathcal{R}$ and $\mathcal{S}$ are identical, but here it makes some sense to differentiate them by taking v to be the drift velocity of our particle, a the particle radius, and T the period of the external drive we will add to the bonds in the following sections. With these definitions, the Reynolds number varies from 10^{-3} to 0.1 and the Stokes number varies from 0.1 to 100. It is clearly the later that gives rise to inertial effects. While these may seem large for a microscopic particle, one should note that there are already experiments in a comparable regime[11].

Coupling between the elastic particle and the fluid is then accomplished through the use of locally applied forces on both the out layer of particle nodes and the fluid according to

$$\mathbf{f} = \pm\gamma\left(\mathbf{v}_p - \mathbf{v}\right), \tag{5}$$

where the + sign corresponds to the force of the node on the fluid, and the − sign corresponds to the force of the fluid on the node. Here, $\mathbf{v}_p$ is the velocity of the node, $\mathbf{v}$ is the local fluid velocity, and γ is chosen in such a way the no-slip boundary condition is reasonably approximated. Full details, along with numerous tests of this method can be found in Refs [24,23,31,29,30,25,1,3,4]

3 Relaxation of externally driven elastic sphere

To understand the behavior of our model, we compared the internal modes of oscillation with continuum mechanical predictions made in recent work by Felderhof [9]. Using the linearized Navier-Stokes (omitting the second term on the left hand side of the second equation in Eq. (1) and assuming the density is constant) Felderhof shows that for a uniform elastic sphere with shear modulus μ and bulk modulus κ submersed in a fluid, the magnitude of the response observed as the result of an external periodic forcing is highly dependent on its frequency. In particular, he shows the magnitude of the response exhibits several resonant peaks at various frequencies, before exhibiting the behavior of a rigid sphere in the low-frequency limit.

In addition to the linearized Naiver-Stokes equations, Felderhof considers an elastic displacement function $\boldsymbol{u}(\boldsymbol{r}, t)$ of a sphere centered at the origin, which is assumed to satisfy the equation of motion [16]

$$\rho_s \frac{\partial^2 \boldsymbol{u}}{\partial t^2} = \mu \boldsymbol{\nabla}^2 \boldsymbol{u} + \left(\frac{1}{3}\mu + \kappa\right) \boldsymbol{\nabla}\boldsymbol{\nabla} \cdot \boldsymbol{u} + \boldsymbol{F}(t) \quad , \tag{6}$$

where ρ_s is the sphere density, μ and κ are bulk and shear modulii, and $\boldsymbol{F}$ is a time-dependent external forcing. The external forcing is assumed to be sinusoidal, as is the response. After Fourier transforming to frequency space, Felderhof derives the relationship

$$\boldsymbol{U}_{\boldsymbol{\omega}} = \left(\frac{3m_f}{4\pi m_p \eta a}\right) \hat{F}_T(x) \boldsymbol{E}_{\boldsymbol{\omega}} \ , \tag{7}$$

where $\boldsymbol{U}_{\boldsymbol{\omega}}$ and $\boldsymbol{E}_{\boldsymbol{\omega}}$ are the center-of-mass velocity of the sphere and the applied external forcing in frequency space respectively, and $\hat{F}_T$ is a dimensionless translational admittance function of complex argument $x = a\left(-i\omega\rho/\eta\right)^{1/2}$. m_p is the mass of the sphere, m_f is the mass of the displaced fluid, and a is the sphere radius. To make the admittance more amenable to analysis it is re-expressed as

$$\hat{F}_T(x) = \frac{1}{x^2 + M Z_T(x)} \ , \tag{8}$$

where $M = \frac{9m_f}{2m_p}$ and Z_T is a function related to the translational friction coefficient between the force applied and the velocity response.

The behavior of Z_T is especially key to understanding the elastic behavior of the model. In the general case, Z_T takes the form

$$Z_T(x) = 1 + x + Z_c x^2 + O(x^3) \ , \tag{9}$$

which in the case of a no-slip rigid sphere reduces to the case $Z_c = 1/9$ with no higher-order terms. For an elastic sphere, Felderhof shows that

$$Z_c = \frac{1}{9} - \frac{\eta}{a\rho}\frac{c_l + c_t}{c_l c_t} + \frac{\eta^2}{a^2\rho}\frac{403\mu + 210\kappa}{180\mu\kappa} \ . \tag{10}$$

where c_l and c_t are velocities related to the elastic constants of the sphere with units of velocity ($c_t = \sqrt{\mu/\rho}$ and $c_l = \sqrt{(3\kappa + 4\mu)/\rho}$). The quantity Z_c itself is dimensionless, but the second and third terms vary inversely with a Reynolds-like number $\mathcal{R}$ (defined by the inverse of the 2nd term) where *the characteristic velocity is now related to* c_l and c_t (i.e *speeds of sound in the elastic* media). For a sphere of radius 1 μm and elastic constants of 10 kPa the second and third terms are an order of magnitude bigger than the first term. Since our setup focuses has a small Reynolds number, a moderate Stokes number and also a moderate value of this new Reynolds-like number, we expect the admittance and friction coefficients to vary dramatically with the fluid and elastic parameters. As we will see, this makes the high frequency response sensitive to the presence of elastic resonances of the system.

To further test this prediction, we conducted a series of simulations to measure $\hat{F}_T$ and compare the behavior of our model to the behavior derived in Felderhof's paper. Using a sphere 1 μm in diameter with fixed equilibrium bond lengths r_0 and a bulk modulus of $B = 9.4$ kPa, we applied a series of sinusoidal forcing at various frequencies to our spherical particle, and plotted the instantaneous motion of its center of mass once the system had reached steady-state behavior. The instantaneous center of mass velocity curve was then fitted to a sinusoidal function of the same frequency as the applied forcing, from which the amplitude of response and phase shift (relative

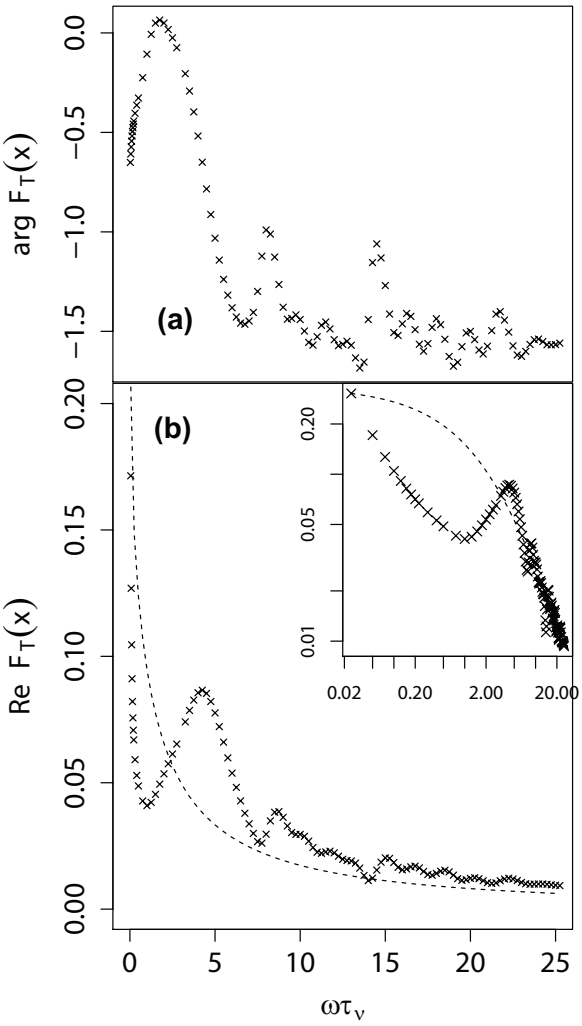

Fig. 1. Measurements of the admittance response function for a uniform elastic sphere as a function of frequency. $\tau_v = a^2/\eta$ is the viscous relaxation time. In (a) we plot the argument (F_T is complex) and (b) gives the Real part of F_T. The simulation data are indicated by symbols and the dotted line gives the function $\hat{F}_T$ for a no-slip rigid sphere. Inset: same data as in (b) but shown using log-log axes.

to the phase of the forcing) was obtained. Using Eq.(7), this allowed us to compute $\hat{F}_T$.

In Figure 1 we plot $\hat{F}_T$ for both a theoretical no-slip rigid sphere and the experimentally determined values from our model as functions of the dimensionless frequency $\omega\tau_v$, where $\tau_v = a^2\rho/\eta$ is the viscous relaxation time. Viewing Figure 1, it is clear there are lots of resonant peaks similar to those predicted by Felderhof's results[9], before approaching the rigid no-slip approximation in the low-($\omega\tau_v$) limit. It is also interesting that for most frequencies the argument of F_T is negative, approaching $-\pi/2$ for high frequencies. It appears that at high frequencies the sphere stores internal elastic energy and releases it later in the cycle. Note that the resonant frequencies of an elastic sphere are $\sim 2\pi a/(c_l\xi)$ where ξ is a solution to a transcendental equation [10]. For our system that places them in the 0.1 to 1 MHz, or periods of 1-10 μs of the drive. Unfortunately, such analysis is only applicable for its qualitative behavior, as accurately modeling the elastic properties of the hcp lattice from which we construct the sphere requires more than two independent elastic constants.

However, despite these limitations there are clear implications from this analysis. As seen above, at high frequencies there are many resonant peaks that depend on both details of the sphere such as its elastic constants as well as details of the fluid such as viscosity. However the long-time behavior of the spheres velocity is found to be[9]

$$\mathbf{U}(t) \approx \frac{1}{12\rho(\pi\mu t/\rho)^{3/2}}\mathbf{E} \tag{11}$$

where $\mathbf{E}$ is the drive amplitude, a result that is independent of the elastic properties of the sphere. The result is: resonant peaks at short periods (high frequency) that depend on the elastic constants of the sphere and a power-law approach to the particle moving with the fluid at low frequencies. This suggests it may not be appropriate to use the period T as a time scale in this regime when the long-time response is related to a power-law (i.e. scale-free: effectively the system does not entirely forget what went on before).

4 Internally driven elastic sphere

To propel the sphere internally, a method of propulsion was devised based on periodically varying the equilibrium bond lengths between constituent particles. Varying bond lengths in this way closely resembles the behavior of piezoelectric materials under external electric fields[15], and is therefore an experimentally realizable approach. The sphere was initially divided into two halves along a plane orthogonal to one of the 6 hcp lattice directions, and the equilibrium bond lengths in Eq.(2), $r_{0,1}$ and $r_{0,2}$ in halves 1 and 2 were varied sinusoidally via the relationship

$$r_{0,i}(t) = L((1-\alpha) + \alpha\sin(\omega t + \phi_i)) \tag{12}$$

where L is the bond length in a unstimulated state, $\alpha \in [0, 0.2]$ such that $(1-\alpha)L$ is the average bond length upon stimulation, and $|\phi_2 - \phi_1| = \pi$. Consequently, the equilibrium bond lengths varied sinusoidally with maximum value L and minimum value $(1-2\alpha)L$, and the variations in the two halves were π radians out of phase with one another. To ensure there is no asymmetry in the sphere, all bonds crossing the mid-plane are left undriven (i.e. fixed r_0). Diagrammatically, the behavior for $\alpha = 1/5$ appears as in Figure 2 (A large value of α is shown in the figure to make the deformation clearer; we used $\alpha \leq 0.1$ in what follows)).

Figure 3 shows the resulting center-of-mass motion of the sphere as a function of time over a large number of periods of the drive for a case where $\alpha = 0.075$. Remarkably, in addition to the oscillatory behavior, the sphere spontaneously breaks symmetry and swims (i.e. attains a net

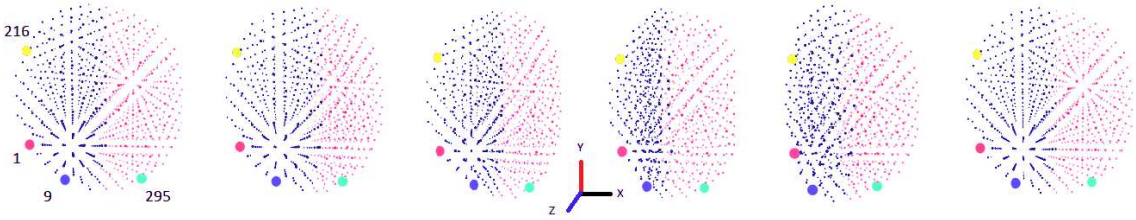

Fig. 2. Deformation of the sphere over the course of one period of oscillation. The two sides of the sphere are colored differently to indicate the different phase of stimulation in Eq.(12) (i.e. one side contracts when the other side expands and vice versa), and four bigger and differently colored particles(marked with IDs - 1,9,216 and 295) on the outer surface which we tracked for further analysis are also indicated. The deformations occur in order from left to right.

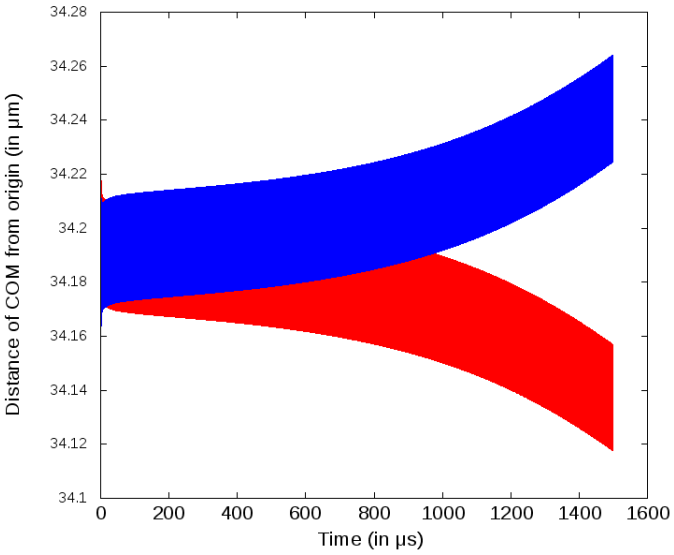

Fig. 3. Center-of-mass motion of a diameter 10 μm sphere with bulk modulus $B = 18.8$ kPa with drive period $\tau = 1$ μs. The sphere was split in half perfectly symmetrically. The only difference between the situation giving rise to the two curves is the initial phase of the drive (i.e. which half of the sphere contracted rather than expanded first). The curves appear as band as the sphere is undergoing many oscillations.

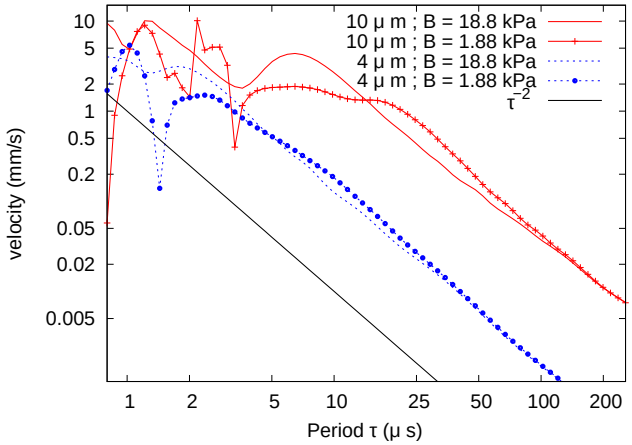

Fig. 4. Log graph of v_{avg} versus τ for $B = 1.88$ kPa & $B = 18.8$ kPa. For short periods, the magnitude of the sphere velocity exhibits many peaks corresponding to the sphere's internal modes of oscillation, before exhibiting power-law behaviour for low driving-frequencies. The average velocities for both spheres overlap at higher periods.

velocity) either to the left or right. The direction chosen appears to depend only on the initial phase of the drive, i.e. the sign of $\phi_2 - \phi_1 = \pm\pi$ in Eq.(12). The result is that, although the driving is periodic, the motion of the sphere not entirely periodic and it picks up a drift in one direction. The motion is analogous to a washing machine becoming off-balance and "walking" across a floor. This motion turns out to be remarkably effective at propelling the particle.

If we introduce a small asymmetry in the sphere by assigning all bonds crossing the mid-plane to one side (right side in Fig 2) we can propel the sphere even faster (almost a factor of 10). The asymmetry also fixes the direction of the final drift velocity of the sphere which now becomes independent of the initial phase. To see how effective the propulsion mechanism is, we measured the average velocity of the particle, v_{avg}, as a function of the oscillation period τ for $\alpha = 1/10$ (10 % variation in bond length). Two different spheres, with diameters 4 μm, and 10 μm were simulated with bulk moduli $B = 1.88$ kPa and $B = 18.8$ kPa, for a total of 4 different datasets. Each dataset contained 110 simulations, each corresponding to a different frequency, where the spherical object was driven by the described propulsion mechanism for 150 periods. The last 10 periods were then used to compute the average velocity of the center of mass.

In Figure 4, we show the average velocity for each of the two spheres as a function of frequency for $B = 1.88$ kPa and $B = 18.8$ kPa. For short periods, the average velocity function exhibits many peaks corresponding to the internal modes of oscillation of each sphere, and shows power-law behavior for low driving-frequencies (longer periods). As the the diameter of the sphere is increased, the average velocity increases. We comment on this behavior more below. Overall, the velocities achieved are remarkably high for such small objects, approaching up to 10 mm/s for short driving periods. While the high-frequency/shortperiod end of the spectrum is outside of something that would be practical for a biological system, it is within the regime that can be constructed artifici-

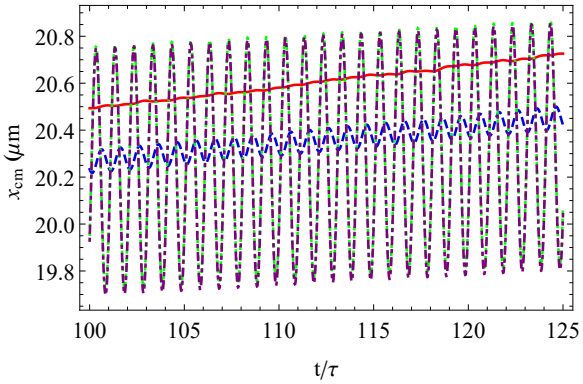

Fig. 5. Center-of-mass motion of a diameter 10 μm sphere with bulk modulus $B = 1.88$ kPa with drive period $\tau = 1$ μs (solid red) and $\tau = 160$ μs (dotted green), and $B = 18.8$ kPa with drive period $\tau = 1$ μs (dashed blue) and $\tau = 160$ μs (dot-dashed purple).

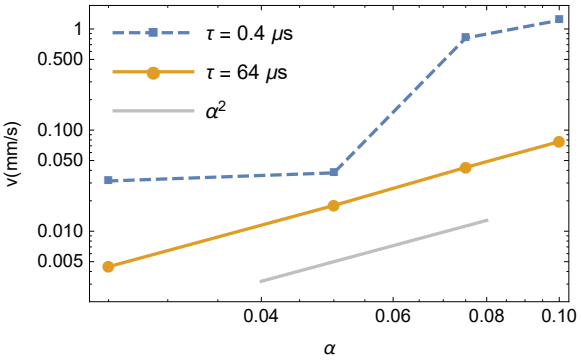

Fig. 6. Average velocity of a diameter 10 μm sphere with bulk modulus $B = 1.88$ kPa with drive periods $\tau = 0.4$ and 64 μs as a function of α. The square of the amplitude of the bond oscillations (cf. Eq.(12)) is shown as a light grey line.

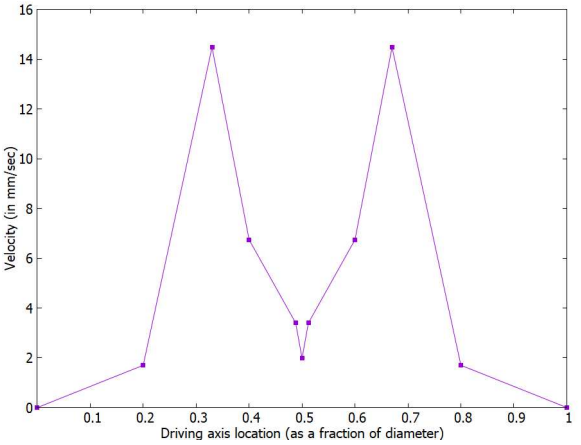

Fig. 7. Average velocity of a diameter 10 μm sphere with bulk modulus $B = 1.88$ kPa with drive period $\tau = 1$ μs as a function of the location of the plane dividing the two sections of the sphere being driven 180° out of phase.

ally (driving of a nanoparticle at more than a million rpm was recently achieved in [11]). In the low kilohertz range, which would be within the range that could be generated by a biological system, the 10 μm sphere still achieves speeds of a few μm/s.

In Figure 4, it can also be seen that the decrease in elastic modulus gives rise to larger peaks and stronger resonance effects, before exhibiting power-law behavior for low driving-frequencies as before. A fit of both diameters and bulk modulus' velocity versus period data in the power-law region gives a dependence of order τ^b with $b = -1.9 \pm 0.1$. Asymptotically, there appears to be an apparent approach to τ^{-2} for larger periods of oscillation. Interestingly, this asymptotic behavior appears to be independent of the stiffness of the sphere and depends only on its diameter. This is similar to the behaviour seen in the previous section for the response function of an externally driven elastic sphere.

The center-of-mass motion of the spheres (once steady motion is achieved) as a function of time, scaled by the period of the drive, is shown in Figure 5 for a few specific cases. While there is oscillations about the linear increase of x_{cm} with time, the amount of oscillation varies considerably. At low drive period (high frequency) the motion is fairly efficient in the sense that the forward movement per period is comparable to the overall amplitude (solid red and dashed blue lines in Fig. 5) whereas at high drive period the sphere advances only a small fraction of its overall amplitude (dotted green and dot-dashed purple lines in Fig. 5). Consistent with the observation with the asymptotic velocities (cf. Fig. 4), the center-of-mass motion at long periods becomes independent of the elastic constant (the dotted green and dot-dashed purple curve in Fig. 5 overlap). However, for short periods the softer (smaller B) sphere has more efficient motion, consistent with its higher velocity in Fig. 4.

Additional simulations examined the effect of the driving amplitude on velocity. As shown in Fig. 6, at longer periods (64 μs in the figure) the mean velocity is proportional to the amplitude squared, suggesting that the motion is a non-linear response to the drive. While the response is well described by the quadratic behavior seen in the figure for most of the range of periods, close to the resonances at shorter period there are considerable deviations, again reflecting the nonlinear response and requiring use of the complete Navier-Stokes description applied here.

As the slightly asymmetric sphere results in higher net swimming speeds than the perfectly symmetric case, it is also worthwhile to vary the division of the sphere. In this case we move the plane dividing the two sections of the sphere from one side to the other. The resulting swimming speeds are shown in Fig 7. The plot is symmetric about the point of even division (0.5) and peaks around a 2/3:1/3 section ratio. The peak is about five times higher than the slightly asymmetric case, giving impressive speeds of 1.4 cm/s for an object only 10 μm in size

5 Detailed Analysis of motion

We performed further analysis on our simulation results to ascertain the means of propulsion and the importance

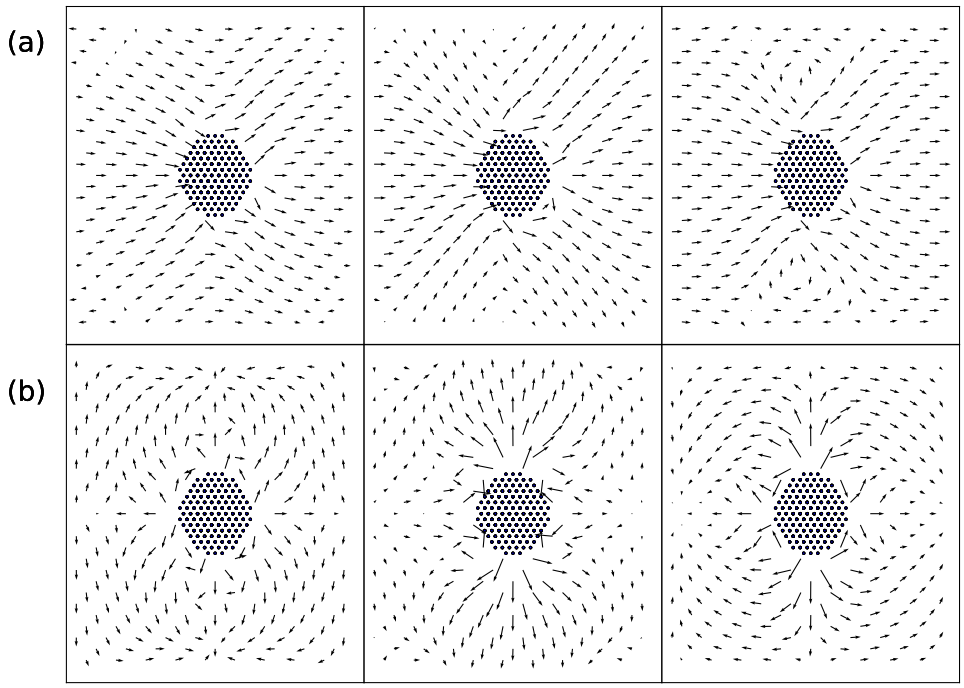

Fig. 8. Fluid flow in the (a) plane cutting through the center of the particle where the motion is left to right and (b) plane cutting through the center of the particle where the motion is coming out of the plane towards the viewer. The slices are at different, equally spaced, points during one period of the motion (after a steady mean velocity has been attained). The length of the velocity vectors have a logarithmic scale. The plots shown are for a 10 μm sphere with $B = 1.88$ kPa with a period of 1 μs (same case as the solid red line in Fig. 5). The equilibrium cross-section of the sphere is shown only schematically (particles making up the real sphere move in and out of the plane during the motion making the dynamic case hard to represent in 2D).

of elasticity and inertia. We first examine the fluid flow that leads to the motion. Figure 8 shows the flow in orthogonal cross-sections of the system at different points in the period of the motion for one particular case. Near the beginning of the cycle (leftmost panels in Fig. 8) the flow field is similar to that of a Stokeslet (force) dipole while later in the cycle it more resembles a source dipole (cf., for example, Fig. 2 in Ref.[36]). The fact that a dipole-like flow field is set up is perhaps not too surprising given the fact that we are driving the two halves of our sphere asymmetrically. As such, the appearance of a resulting dipole moment would seem hard to avoid.

However, if the bonds exactly followed the drive, the Scallop Theorem would still suggest no steady velocity would be achieved as the motion would be reciprocal. Here our object is elastic, which allows the bonds to lag (or lead) the drive, and we are using the full Navier-Stokes equations, rather than the Stokes approximation, so in addition to non-reciprocal motion we can also see any inertial effects.

Firstly, we examine how the periodic driving of the harmonic bonds results in a global periodic deformation of the sphere. To do this, we selected four constituent particles (represented by numeric IDs - 1, 9, 216, and 295; see Figure 2) on the surface of the 10 μm sphere, with $B = 18.8$ kPa, in the $z = 0$ plane, and analyzed their position from the sphere's center of mass as a function of time.

The location of these constituent particles is depicted in Figure 2. Particles 1 and 216 are colored as red and yellow respectively. Particles 9 and 295 are colored as blue and green respectively. To test whether there was any non-reciprocal motion, we ran simulations of the 10 μm sphere driven with a period of 0.8 μs and, for comparison, also at a period of 50 μs. In each case we computed the position of each particle relative to the center of mass of the sphere at each timestep. The sphere was driven for 150 periods and the first 25 were ignored to only track the particles once the sphere had attained stable motion. The path traced by the location of the particles with respect to that of the center of mass of the sphere is presented in Figure 9. Note that in Figure 9 the motion is shown in the $xy-$plane because there is negligible movement along the $z-$axis.

As can be seen in Figure 9, particles 1,9,216 and 295 all move in a loop with respect to the center of mass of the sphere, which clearly shows that the movement is periodic

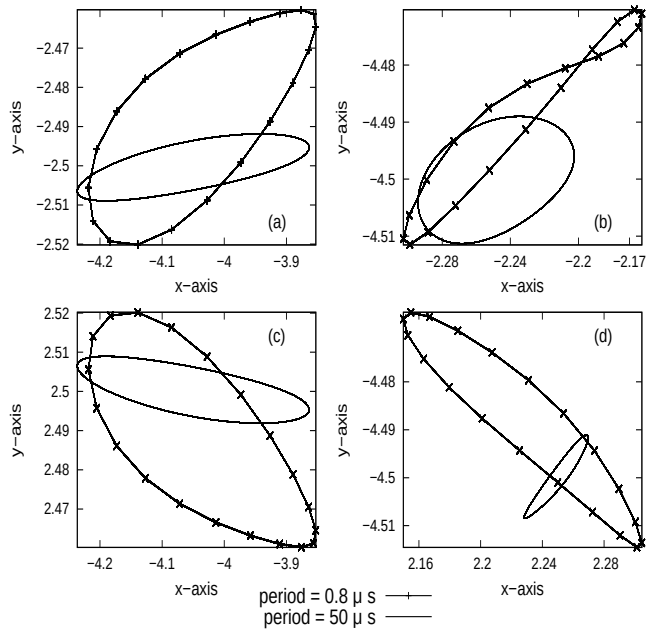

Fig. 9. Comparison of motion of outer particles (IDs 1,9,216 and 295 as depicted in Figure 2), with respect to center of mass of spheres of diameter 10 μm with $B = 18.8$ kPa, driven at periods of 0.8 μs and 50 μs. Fig.(a) shows particle 1's track , Fig.(b) shows particle 9's track, Fig.(c) shows particle 216's track and Fig.(d) shows particle 295's track.

(the motion is plotted over multiple periods of the drive so the fact that a single closed loop is observed indicates that the motion is periodic). The presence of two-dimensional open loops (as opposed to one-dimensional curves) indicates that the motion of the surface is non-reciprocal (i.e. the particles do not retrace their path in time when moving from their maximum to minimum extent during a single period of the motion). Notice how the amplitude of deformation is somewhat smaller for the sphere driven at higher (50 μs) period, due to absence of the resonance effect that occurs at shorter periods. This change in deformation is, however, nowhere near the more than order of magnitude difference in the sphere velocities for these two periods (cf. Fig. 4). However, considering that the amplitude of the bond-length change during one period is the same for both cases, the fact that the amplitude of the motion of surface nodes is similar is not that surprising. This again means that the time-dependent terms in Navier-Stokes are essential for the motion (the only difference between the two cases shown in the figure is the period of the drive). The periodic movement of these outer particles is also consistent with the observed dipole-like flow seen in Figure 8, although the loop crossing seen in Fig. 9(b) suggests the potential presence of a small quadrapole moments in the outer surface of the sphere over a period of the motion. We note that although the surface deformation is non-reciprocal, it is not consistent with motions like the "flexible-oar" strategy where a traveling wave along a filament produces propulsive force[22,39,41]. In this case the flow field demonstrates dipole-like behavior and the mean sphere velocity is not linearly proportional to the amplitude of the driving (as seen in Fig. 6) or the amplitude of the surface deformation and does not fit within the Stokes approximation used in the Scallop Theorem.

Secondly, we investigated the contribution of inertial forces to the driving of sphere. We used the simulation data with the sphere of diameter 10 μm and bulk modulus B = 18.8 kPa. To do this, we compared the inertial forces to those arising from the ∇p term in Eq.(1). We first integrated these forces throughout the *exterior volume*, which is basically the entire volume of simulation box, minus the volume inside a sphere centered on the center of mass of the sphere but with a radius four lattice points larger than the radius of the relaxed sphere. The shell of four grid points from the surface of sphere was excluded from the total volume to avoid the fluctuating parts of the sphere in the external volume where forces are integrated. To get the inertial forces, we integrated the absolute value of terms on the left hand side of Navier-Stokes equation (1). To get the forces from the pressure gradient, the absolute value of ∇p was integrated throughout the exterior volume. For calculating all the derivatives (both space and time), forward differences were used.

The result has been plotted in Figure 10 along with the velocity profile of the driven sphere. It can be seen that inertial forces are *dominant* in the low driving period (high frequency) region, where the overall velocity is also high. However, in the large driving period (low frequency) region the inertial forces are considerably smaller, approaching a tenth of the ∇p forces at longer periods. This leads to the question of whether inertial forces are ever truly negligible. For low periods inertial forces are clearly significant and for longer periods, even though their magnitude is much smaller, the power law tail of the mean velocity is likely related to the hydrodynamic power-law tail seen in linear response. As the hydrodynamic tail is intrinsically related to the inertia of the fluid, even at long periods, it would seem that the inertia is important for the mean velocity, even if it is considerably smaller than other terms in Navier-Stokes.

6 Conclusions

Through computer simulation of an elastic spherical particle in a Lattice-Boltzmann fluid, we have shown that it is possible to drive internal elastic modes of oscillation to produce swimming motion and that inertia is a significant element. In particular, we found that by varying the bond lengths of a spherical particle sinusoidally, we were able to produce propulsion. This is different from elastic bead-spring models with a few constituent particles, such as the one discussed by Ledesma-Aguilar [18], that lack the internal degrees of freedom of a larger, more flexible three-dimensional object consisting of several hundred particles such as ours. In our case, even though the drive is reciprocal, the elastic modes excited in the sphere result in periodic but non-reciprocal motion of the sphere's surface,

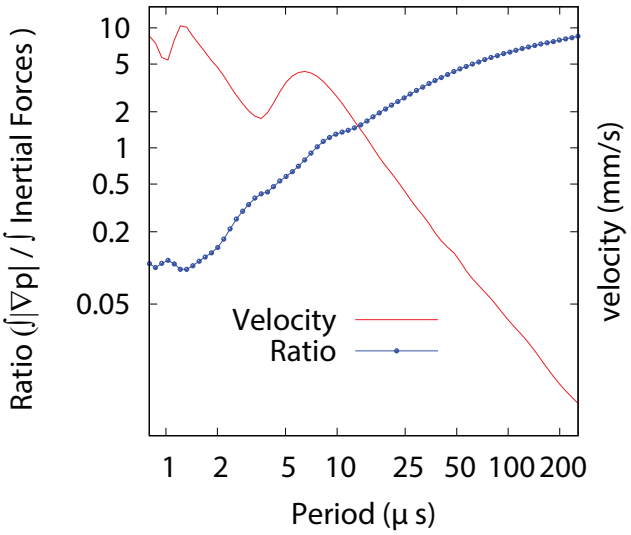

Fig. 10. Log graph showing comparison of variation of ratio of elastic to inertial forces in the system w.r.t driving period (in μs), and variation of velocity (in mm/s) w.r.t. driving period (in μs) for sphere with 10 μm diameter and bulk modulus B = 18.8 kPa.

driving dipole-like flow fields in the fluid. At high frequencies, the speeds obtained by are model are very high, in the mm/s range, and even at low frequencies the particles can move several body lengths per second. At high frequencies the magnitude of inertial terms is comparable to other terms in Navier-Stokes and is therefore non-negligible. Even at low frequencies where inertial terms are relatively small, the net propulsion is still likely only possible due to their presence.

High frequency driving (more than a million rpm) of nanoparticles has recently been demonstrated in light-driven submersible nanomachines[11] and the speeds obtained by our model are comparable for a much wider range of particle sizes. In particular, current technology should be capable of creating microparticles with the properties of our model which could be used to replicate this behavior by stimulation using an external electric field.

7 acknowledgments

This work was supported by the Natural Science and Engineering Council of Canada (NSERC). Computational resources were provided by the Shared Hierarchical Academic Research Computing Network (SHARCNET), and Compute/Calcul Canada.

8 Authors contributions

All the authors were involved in the preparation of the manuscript. All the authors have read and approved the final manuscript.

References

1. M. M. T. Alcanzare, V. Thakore, S. T. T. Ollila, M. Karttunen, and T. Ala-Nissila. Controlled propulsion and separation of helical particles at the nanoscale. *Soft Matter*, 13:2148–2154, 2017.
2. B. J. Alder and T. E. Wainwright. Decay of the velocity autocorrelation function. *Phys. Rev. A*, 1:18–21, Jan 1970.
3. A. Antipova and C. Denniston. Dynamics of a disc in a nematic liquid crystal. *Soft Matter*, 12:1279–1294, 2016.
4. A. Antipova and C. Denniston. Dynamics of disk pairs in a nematic liquid crystal. *Phys. Rev. E*, 94:052704, Nov 2016.
5. N. Aschcroft and N. Mermin. *Solid State Physics*. Saunders College, 1976.
6. A. M. Colinsworth, S. Zhang, W. E. Kraus, and G. A. Truskey. Apparent elastic modulus and hysteresis of skeletal muscle cells throught differentiation. *American Journal of Cell Physiology*, 283:C1219 to C1227, 2002.
7. D. Di Carlo. Inertial microfluidics. *Lab Chip*, 9:3038–3046, 2009.
8. R. Dreyfus, J. Baudry, M. Roper, M. Fermigier, H. Stone, and J. Bibette. Microscopic artificial swimmers. *Nature*, 437:862–865, Oct 2005.
9. B. U. Felderhof. Jittery velocity relaxation of an elastic sphere immersed in a viscous incompressible fluid. *Physical Review*, 89:033001, 2014.
10. V. Galstyan, O. S. Pak, and H. A. Stone. A note on the breathing mode of an elastic sphere in newtonian and complex fluids. *Physics of Fluids*, 27(3):032001, 2015.
11. V. García-López, P.-T. Chiang, F. Chen, G. Ruan, A. A. Martí, A. B. Kolomeisky, G. Wang, and J. M. Tour. Unimolecular submersible nanomachines. synthesis, actuation, and monitoring. *Nano Letters*, 15(12):8229–8239, 2015. PMID: 26540377.
12. M. Habibi, C. Denniston, and M. Karttunen. Micelle fragmentation and wetting in confined flow. *EPL (Europhysics Letters)*, 108(2):28005, 2014.
13. E. Hauge and A. Martin-Löf. Fluctuating hydrodynamics and brownian motion. *Journal of Statistical Physics*, 7:259, 1972.
14. B. P. Ho and L. G. Leal. Inertial migration of rigid spheres in two-dimensional unidirectional flows. *Journal of Fluid Mechanics*, 65:365–400, 8 1974.
15. Landau and Lifshitz. *Electrodynamics of Continuous Media*. Pergamon Press, 1960.
16. L. D. Landau and E. Lifshitz. *Theory of Elasticity*. Pergamon Press, 1959.
17. E. Lauga. Life around the scallop theorem. *Soft Matter*, 7:3060–3065, 2011.
18. R. Ledesma-Aguilar, H. Löwen, and J. M. Yeomans. A circle swimmer at low reynolds number. *The European Physical Journal E*, 35(8):70, 2012.
19. A. Lindner and M. Shelley. Elastic fibers in flows. *Fluid-Structure Interactions in Low-Reynolds-Number Flows*, pages 168–192, 2015.
20. M. Loferer-Krößbacher, J. Klima, and R. Psenner. Determination of bacterial cell dry mass by transmission electron microscopy and densitometric image analysis. *Applied and Environmental Microbiology*, 64(2):688–694, 1998.
21. A. J. Mach, J. H. Kim, A. Arshi, S. C. Hur, and D. Di Carlo. Automated cellular sample preparation using a centrifuge-on-a-chip. *Lab Chip*, 11:2827–2834, 2011.

22. K. Machin. Wave propagation along flagella. *J. Exp. Biol.*, 35:796, 1958.
23. F. Mackay and C. Denniston. Coupling {MD} particles to a lattice-boltzmann fluid through the use of conservative forces. *Journal of Computational Physics*, 237:289 – 298, 2013.
24. F. Mackay, S. T. T. Ollila, and C. Denniston. Hydrodynamic forces implemented into lammps through a lattice-boltzmann fluid. *Computer Physics Communications*, 184:2021 to 2031, 2013.
25. F. E. Mackay, K. Pastor, M. Karttunen, and C. Denniston. Modeling the behavior of confined colloidal particles under shear flow. *Soft Matter*, 10:8724–8730, 2014.
26. M. Masaeli, E. Sollier, H. Amini, W. Mao, K. Camacho, N. Doshi, S. Mitragotri, A. Alexeev, and D. Di Carlo. Continuous inertial focusing and separation of particles by shape. *Phys. Rev. X*, 2:031017, Sep 2012.
27. J. L. McWhirter, H. Noguchi, and G. Gompper. Deformation and clustering of red blood cells in microcapillary flows. *Soft Matter*, 7:10967–10977, 2011.
28. H. Noguchi and G. Gompper. Swinging and tumbling of fluid vesicles in shear flow. *Phys. Rev. Lett.*, 98:128103, Mar 2007.
29. S. T. T. Ollila, C. Denniston, and T. Ala-Nissila. One- and two-particle dynamics in microfluidic t-junctions. *Phys. Rev. E*, 87:050302, May 2013.
30. S. T. T. Ollila, C. Denniston, M. Karttunen, and T. Ala-Nissila. Biopolymer filtration in corrugated nanochannels. *Phys. Rev. Lett.*, 112:118301, Mar 2014.
31. S. T. T. Ollila, C. J. Smith, T. Ala-Nissila, and C. Denniston. The hydrodynamic radius of particles in the hybrid lattice boltzmann–molecular dynamics method. *Multiscale Model Simul.*, 11:213–243, 2013.
32. S. Plimpton. Fast parallel algorithmns for short-range molecular dynamics. *J Comp Phys*, 117:1 to 19, 1995.
33. E. Purcell. Life at low reynolds number. *American Journal of Physics*, 45:3 to 11, 1977.
34. T. Qiu, T.-C. Lee, A. Mark, K. Mrozov, R. Mnster, O. Mierka, S. Turek, A. Leshansky, and P. Fischer. Swimming by reciprocal motion at low reynolds number. *Nature Communications*, 5:5119, 2014.
35. G. SEGR and A. Silberberg. Radial particle displacements in poiseuille flow of suspensions. *Nature*, 189:209, 1961.
36. S. E. Spagnolie and E. Lauga. Hydrodynamics of self-propulsion near a boundary: predictions and accuracy of far-field approximations. *Journal of Fluid Mechanics*, 700:105147, 2012.
37. E. D. Tytell, C.-Y. Hsu, T. L. Williams, A. H. Cohen, and L. J. Fauci. Interactions between internal forces, body stiffness, and fluid environment in a neuromechanical model of lamprey swimming. *Proceedings of the National Academy of Sciences*, 107(46):19832–19837, 2010.
38. E. D. Tytell, M. C. Leftwich, C.-Y. Hsu, B. E. Griffith, A. H. Cohen, A. J. Smits, C. Hamlet, and L. J. Fauci. Role of body stiffness in undulatory swimming: Insights from robotic and computational models. *Phys. Rev. Fluids*, 1:073202, Nov 2016.
39. C. H. Wiggins and R. E. Goldstein. Flexive and propulsive dynamics of elastica at low reynolds number. *Phys. Rev. Lett.*, 80:3879–3882, Apr 1998.
40. W.-C. Yeh, P.-C. Li, Y.-M. Jeng, H.-C. Hsu, P.-L. Kuo, M.-L. Li, P.-M. Yang, and P. H. Lee. Elastic modulus measurements of human liver and correlation with pathology. *Ultrasound in medicine and biology*, 28:467 to 474, 2002.
41. T. S. Yu, E. Lauga, and A. E. Hosoi. Experimental investigations of elastic tail propulsion at low reynolds number. *Physics of Fluids (1994-present)*, 18(9):091701, 2006.
42. R. Zwanzig and M. Bixon. Hydrodynamic theory of the velocity correlation function. *Phys. Rev. A*, 2:2005–2012, Nov 1970.